# Two Tonoplast Proton Pumps Function in Arabidopsis Embryo Development

Yu-Tong Jiang[1], Ren-Jie Tang[2], Yan-Jie Zhang[1], Hong-Wei Xue[3, 4], Ali Ferjani[5], Sheng Luan[2*] and Wen-Hui Lin[1, 2*]


[1]School of Life Sciences and Biotechnology, The Joint International Research Laboratory of Metabolic & Developmental Sciences, Shanghai Jiao Tong University, 200240 Shanghai, China

[2]Department of Plant and Microbial Biology, University of California, 94720 Berkeley, CA, USA,

[3]School of Agriculture and Biology, Shanghai Jiao Tong University, 800 Dongchuan Road, Shanghai 200240, China.

[4]National Key Laboratory of Plant Molecular Genetics, CAS Center for Excellence in Molecular Plant Sciences, Institute of Plant Physiology and Ecology, Chinese Academy of Sciences, 200032 Shanghai, China

[5]Department of Biology, Tokyo Gakugei University, 184-8501 Koganei-shi, Japan

[*]These authors contributed equally in this work. Correspondence and requests for materials should be addressed to W-H. L. (Tel: +86-21-34208262; email: whlin@sjtu.edu.cn) and Sh. L. (Tel: +1-510-642-6306; email: sluan@berkeley.edu)




ORCID information
Wen-Hui Lin: https://orcid.org/0000-0003-0600-6107
Sheng Luan: https://orcid.org/0000-0002-8375-8276
Hong-Wei Xue: https://orcid.org/0000-0002-7641-5320
Ali Ferjani: https://orcid.org/0000-0003-1157-3261




Individual WeChat account
Wen-Hui Lin: LinWenhui77

## Summary

● Two types of tonoplast proton pumps, $H^+$-pyrophosphatase (V-PPase) and the $H^+$-ATPase (V-ATPase), establish the proton gradient that powers molecular traffic across tonoplast thereby facilitating turgor regulation and nutrient homeostasis. However, how proton pumps regulate development remains unclear.

● In this study, we investigated the function of two types of proton pumps in Arabidopsis embryo development and pattern formation. While disruption of either V-PPase or V-ATPase had no obvious effect on plant embryo development, knocking out both resulted in severe defects in embryo pattern formation from the early stage.

● While the first division in wild type zygote was asymmetric, a nearly symmetric division occurred in the mutant, followed by abnormal pattern formation at all stages of embryo development. The embryonic defects were accompanied by dramatic differences in vacuole morphology and distribution, as well as disturbed localization of PIN1. The development of mutant cotyledons and root, and the auxin response of mutant seedlings supported the hypothesis that mutant lacking tonoplast proton pumps were defective in auxin transport and distribution.

● Taking together, we proposed two tonoplast proton pumps are required for vacuole morphology and PIN1 localization thereby controlling vacuole and auxin related developmental processes in Arabidopsis embryos and seedlings.

**Key words:** V-ATPase, V-PPase, vacuole, auxin, cotyledons.

## INTRODUCTION

Vacuoles play a central role in plant growth and development. They are lytic compartments as well as primary reservoirs for nutrients and metabolites. The central vacuole in a mature plant cell is held together by a membrane referred to as "tonoplast". Arrays of transport proteins reside in the tonoplast to transport ions and solutes inside and outside of the vacuole to maintain a proper turgor pressure and nutrient homeostasis of the cell. Molecular fluxes across the tonoplast are mainly energized by two types of primary proton pumps, the vacuolar $H^+$-ATPase (V-ATPase) and the vacuolar $H^+$-pyrophosphatase (V-PPase) (Neuhaus and Trentmann, 2014). These two abundant proteins cooperate to generate the membrane potential and proton gradient across the tonoplast essential for secondary transport processes. In Arabidopsis, there are three genes encoding $H^+$-pyrophosphatase, which are divided into type I (AVP1/ATVHP1;1/FUGU5) and type II (AVP2;1 and AVP2;2) (Drozdowicz and Rea, 2001). Among these genes, only type I (AVP1/ATVHP1; 1/FUGU5, AT1G15690) is located in the tonoplast (Gaxiola *et al*., 2001; Maeshima, 2001; Segami *et al*., 2010). Genetic analysis of Arabidopsis *avp1* mutants suggests that AVP1 plays a role in several physiological processes, such as seedling growth, gluconeogenesis and high magnesium tolerance, which may be mainly contributable to its pyrophosphatase activity but independent of $H^+$-translocation (Ferjani *et al*., 2011; Yang *et al*., 2018). A recent study supports the idea that AVP1 and V-ATPase both contribute to vacuolar acidification in Arabidopsis (Kriegel *et al*., 2015). V-ATPases are multi-subunit proton pumps comprised of the peripheral $V_1$ complex responsible for ATP hydrolysis and the integral membrane $V_0$ complex in charge of proton translocation (Nishi and Forgac, 2002; Sze *et al*., 2002; Nelson, 2003; Cipriano *et al*., 2008). In plant cells, V-ATPases are not only found in the tonoplast but also present in the trans-Golgi network/early endosome (TGN/EE) (Herman *et al*., 1994; Oberbeck *et al*., 1994). Three distinct isoforms of the $V_0$ subunit (including VHA-a1,2,3) are encoded in Arabidopsis genome and two of them, VHA-a2 (AT2G21410) and VHA-a3 (AT4G39080), are exclusively targeted to the tonoplast,

81  whereas VHA-a1 (AT2G28520) only resides in the TGN/EEs and the deletion mutant

82  of *VHA-a1* is lethal (Dettmer *et al*., 2006). Therefore, the Arabidopsis *vha-a2 vha-a3*

83  double mutant that lacks both of the tonoplast-localized $V_0$ isoforms should be null in

84  tonoplast V-ATPase function (Krebs *et al*., 2010). Interestingly, in contrast to the

85  *vha-a1* single mutant that is lethal, *vha-a2 vha-a3* double mutant remains viable and

86  developmentally normal although it is stunted in growth possibly due to defects in

87  nutrient homeostasis (Krebs *et al*., 2010). More surprisingly, the triple mutant, *vha-a2*

88  *vha-a3 avp1* lacking both tonoplast V-ATPase and V-PPase activities, is viable and

89  retains some vacuolar acidification capacity, suggesting that other players may

90  additively contribute to the pH gradient across the tonoplast (Kriegel *et al*., 2015).

91      During the initial phase of functional analysis of AVP1, a study links AVP1

92  function with auxin-regulated plant development (Li *et al*., 2005). However, a later

93  study (Kriegel *et al*., 2015) demonstrated that the mutant *avp1-1* used in Li *et al* (2005)

94  contains a mutation in *GNOM* (Steinmann *et al*., 1999; Geldner *et al*., 2001) gene,

95  leading to the observed auxin-related phenotypes. During our study on the functional

96  relationship of AVP1 and V-ATPase, we also confirmed that *avp1* single mutant

97  failed to show auxin-related defects. However, we discovered that when both AVP1

98  and V-ATPase were disrupted, the mutant plants showed severe defects in

99  auxin-regulated developmental processes. In our study, a series of previously

100  unreported phenotypes in the *vha-a2 vha-a3 avp1* triple mutant were identified, which

101  were clearly connected to vacuole morphology and auxin signaling in the context of

102  plant embryogenesis and development. Two different alleles lacking both tonoplast

103  V-ATPase and V-PPase (hereafter, the "*vha-a2 vha-a3 avp1*" allele was designated as

104  "*vap3*" and the "*vha-a2 vha-a3 fugu5-1*" allele was designated as "*fap3*"), but not any

105  single or double mutants, displayed severe growth defects in embryo development and

106  seedling establishment. The defects in the triple mutants lacking both pumps were

107  reminiscent of those observed in mutants defective in auxin transport or signaling.

108  Indeed, further experiments using various transgenic auxin marker lines suggested

109  that those auxin-related developmental phenotypes were correlated with the

110  impairment in overall auxin level, auxin polar transport, and distribution. In particular,

the key auxin exporter PIN1 was mis-regulated in the mutants at multiple levels including protein abundance, exocytosis, and polar localization, which could account for the severe defects in embryo pattern formation, seedling development, and auxin responses in the mutants. Taken together, our results had linked the function of vacuolar proton pumps to auxin-regulated developmental processes.

## Materials and Methods

### Plant Materials and Growth Conditions

All Arabidopsis plants were grown in soil under greenhouse conditions (22 ℃; 16-/8-h light-dark cycle for long day) or on 1/2 MS medium (Murashige and Skoog, 1962) containing 2% sucrose and 0.75% agar in the growth chamber (22 ℃/18 ℃; 16-/8-h light-dark cycle). The wild type control used in this study was Col-0 ecotype and all of our plant materials were in Col-0 background. The *avp1* mutant corresponded to the T-DNA insertion line GK-596F06-025557 from Luan lab (Yang *et al*., 2015). The primers for genotyping are: AVP1-747F, 5'-TGGGATCTACACTAAGGCTGCTG-3' and AVP1-1268R, 5'-CCAATAATGAGTCCAGCCCAAAG-3'). c primers for genotyping: forward, 5'-CAGGCTGGTGTATCAGAGCAT-3' and reverse, 5'-GACTCAACAGCCATGAGCTT-3'). The *vha2* mutant was constructed by two T-DNA insertion lines *vha-a2* (SALK_142642) and *vha-a3* (SALK_029786) from Salk Institute for Biological Studies, and identified by genotyping (primers: VHA-a2-LP, 5'-GCAACTCGTTCAAGTCATTG-3' and VHA-a2-RP 5'-ACCGCTGCAACTTGTCGTTA-3'; VHA-a3-LP 5'-CGATGGATCTGATGCGTTCAG-3' and VHA-a3-RP 5'-AGCATGAATGTACCTGTGCTG-3'). The transgenic lines: *pPIN1::PIN1-EYFP* (Xu *et al*., 2006) and DR5::GUS (Sabatini *et al*., 1999) were from Ben Scheres lab. We crossed these two marker line with mutants *avp1*, *vha2* and *vap3* and named them as PIN1-EYFP *avp1*, PIN1-EYFP *vha2*, PIN1-EYFP *vap3* and DR5::GUS *avp1,* DR5::GUS *vha2,* DR5::GUS *vap3*.

140

## Root Gravitropism Assay

The sterilized seeds were sown on 1/2 MS medium containing 2% sucrose. The 7-DAG (day after germination)-seedlings in similar size (average root length) were transferred to 1/2MS medium containing 2% (w/v) sucrose and 0.85% agar. The position of the root apex was marked on the back of the plates, and then the plates were rotated by 90° for gravitropism assay. Images were captured every 2 h by digital camera (Canon D60). Image J was used (http://rsbweb.nih.gov/ij/download.html) to analyze the tip angle (the angle between root tips and the horizontal direction).

149

## Chemical treatment

The 5-DAG-seedlings were transplanted to the vertical plates with 1/2MS medium containing 0.1 μM and 0.5 μM 1-naphthylacetic acid (NAA, Sigma 317918) and 10 μM N-(1-Naphthyl)phthalamic acid (NPA, Sigma 399728). The 5-DAG-seedlings were vacuum fixed (0.5 MPa pressure for 30 minutes) in 4% Polyoxymethylene (PFA, Sigma 158127) solution. After washing three times with PBS solution (NaCl 8 g, KCl 0.2 g, $Na_2HPO_4$ 1.42 g, $KH_2PO_4$ 0.27 g, 1 L, pH = 7.4), the seedlings were cleared into Clearsee solution, which is prepared as described by Kurihara (Kurihara *et al*., 2015). BCECF/AM was used as staining agent to visualize vacuole morphology and to measure vacuolar pH as previously described (Viotti *et al*., 2013).

160

## Histological and fluorescent staining

The root staining experiment requires applying vacuum for half an hour in 4% PFA (paraformaldehyde) solution diluted with PBS (containing 1% triton). Fluorescent Brightener 28 (FB28, Sigma F3543) was used as staining agent for roots' cell walls, which was diluted in 2% (w/v) Clearsee solution. After 3 minutes staining, the roots were washed in Clearsee solution three times and sealed under coverslips. β-glucuronidase (GUS) activity was detected by histochemical staining of tissues at 37 ℃ for 6h and bleaching by 75% alcohol. The GUS stained cotyledons were

169  examined under stereomicroscope (Leica S8APO) and digital images were captured

170  using Leica DFC450. Brefeldin A (BFA, Sigma 203729) treatment was performed in

171  conjunction with FM4-64 (Sigma F34653) staining. After incubation in FM4-64

172  solution (4 μM in 1/2MS liquid medium) for 5 minutes, 5-DAG-seedlings were

173  carefully washed in 1/2 MS liquid medium with tweezers for three times, the

174  seedlings were immersed in BFA treatment solution (50 μM in 1/2MS liquid medium)

175  for 50 minutes before observation. The process of confocal laser scanning microscopy

176  (CLSM) was to draw on Christensen's paper (Christensen *et al*., 1997). We dissected

177  the pistils by first removing the sepals, petals and stamens from isolated flowers. Then

178  we cut the stigma of pistils use a needle of a milliliter syringe under the stereoscope

179  and gently drew two scratches on pistil walls. The pistils were immersed in a solution

180  of 4% glutaraldehyde and 12.5 mM cocadylate for at least 4 hours after applying

181  vacuum for 45 min. Then the tissue was dehydrated in 10%, 30%, 50%, 70%, 80%,

182  90%, 95% ethanol for 10 min each. After immersed in 95% ethanol for 12 h, the

183  tissue was cleared in a 2:1 mixture of benzyl benzoate: benzyl alcohol for 2 h. Then

184  we peeled the seeds out of the pistils and soaked them in Leica Immersion oil

185  11513859 for 2 h and sealed under coverslips.

186

## Confocal Imaging

188  Embryos for fluorescence observation were separated from siliques in each

189  developmental stage. The root we observed separated from 5-DAG-seedlings which

190  vertically growth in 1/2 MS medium with 2% sucrose. Samples were fixed, cleaned

191  and dyed. Then the images were captured by the confocal microscope (Leica/TCS

192  SP8 STED 3X) with a 63 x oil objective. For the detection of PIN1-EYFP, the

193  excitation wavelength was 515 nm and the emission wave length was between 525

194  nm to 575 nm. For the detection of FB28 staining, the excitation wavelength was 405

195  nm and the emission wavelength was between 450 nm to 500 nm. For the detection of

196  CLSM staining, the excitation wavelength was 488 nm and the emission wavelength

197  was between 525 nm to 555 nm. The intensity of the argon ion laser is 8% and

198     Activate STED is 50. Fluorescence intensity statistics used Image J software

199     (http://rsbweb.nih.gov/ij/ download.html).

200

## Scanning Electron Microscopy (SEM)

202     For embryo observation, we soaked the dried seeds for twenty minutes and peeled

203     the seed coats with tweezers carefully. For seedlings' cotyledons observation, we use

204     the 6-DAG-seedlings. Samples were fixed in FAA solution (Anhydrous ethanol: 37%

205     formaldehyde: glacial acetic acid: distilled water = 10: 2: 1: 7, v/ v/ v/ v) by 0.6 MPa

206     for 20 minutes. The materials were sealed and stored at 4 ℃ for 7 days before

207     gradient alcohol dehydration (50%, 60%, 70%, 80%, 90%, 95%, 100% $C_2H_5OH$; each

208     concentration for 15 minutes, the last 100% concentration repeated three times). After

209     dried by Automated Critical Point Dryer (Leica/CPD 300), the materials were coated

210     with gold particles for 20 minutes. Coated samples were transferred to an SEM

211     (Hitachi/S3400II) for examination.

212

## Vacuole extraction

214     We used the rosette leaves of 35-DAG-seedlings as the material for extracting the

215     vacuoles. Take 1 g fresh rosette leaves and slice them into 2 mm pieces using a razor

216     blade. Our method of vacuole extraction is same as previous paper (Robert *et al*.,

217     2007). We extracted the protoplasts with protoplast enzyme solution and washed them

218     gently with wash buffer. Then the protoplasts were disrupted by pre-warmed lysis

219     buffer and the vacuoles could be inspect under Leica DFC450. The solution of

220     vacuole was overlaid with 3 ml 4% Ficoll solution and 1 ml ice-cold vacuole buffer.

221     After Spinning for 50 min at 71,000g at 10 °C, vacuoles should be visible between 0

222     and 4% Ficoll.

223

## Real-Time Quantitative RT-PCR

225     To detect the transcription levels of *AVP1, VHA-a2, VHA-a3* and *CUCs* genes in

226    Col and *vap3* seedlings, cotyledons of 5-DAG-seedlings were collected and total RNA

227    was extracted using Trizol reagent (Invitrogen 10296010), and then

228    reverse-transcripted by FastKing RT Kit（With gDNase） (KR116). The primers using

229    in qRT-PCR were followed. *AVP1*: forward, 5'-CTGTCATTGCTGATAATGTCGG-3'

230    and reverse, 5'-GATTCCCATTGAACTGATGAGC-3'. *VHA-a2:* forward, 5'-

231    GCAACATCTTCATACGACAGTC-3'                    and                    reverse,

232    5'-ACCTGAAACCTCAGTCATCATT-3'.                *VHA-a3:*                forward,

233    5'-CATGCTTAGTCTTGATGTGACG-3'                    and                    reverse,

234    5'-ACTCTTTGGTTCTTAGGACCTG-3'. *ACTIN2* gene was used as a positive

235    internal control with followed primers: forward, 5'-CCTTCGTCTTGATCTTGCGG-3'

236    and reverse, 5'-AGCGATGGCTGGAACAGAAC-3'.   Quantitative RT-PCR was

237    conducted by Eppendorf realplex 4s using SYBR$^{®}$ Green Realtime PCR Master Mix

238    and analyzed by △△threshold cycle (CT) method.

239

240    **SDS-PAGE and Immunoblotting**

241        The material was the root of 6-DAG-seedlings, and the root was cut with scissors

242    along a uniform height. PIN1 protein was analyzed by SDS-PAGE and subsequent

243    immunoblotting. After gel electrophoresis, the proteins were transferred to a

244    nitrocellulose membrane (Whatman). The primary antibody against the PIN1 and

245    TUBULIN A was from Abmart. The secondary antibodies of PIN1 was anti-rabbit

246    IgG (Abmart) and secondary antibodies of TUBULIN A was anti-mouse IgG (H+L)

247    (Abmart). Immunostained bands were analyzed using a CCD camera system

248    (Bio-rad).

249

250    **Phytohormone targeted metabolome analysis**

251        This experiment used UPLC-ESI-MS/MS analysis method to qualitatively detect

252    auxin in samples. We took 2 g fresh leaves from 21-DAG-seedlings' rosette leaves

253    and lyophilized them in Lyophilizer (labconco & Freezone 6PLUS). Then add 500 μL

254    treatment solution (Isopropyl alcohol: water: FA = 2: 1: 0.002) in 14 mg lyophilized

255    sample and grind with 2 steel balls (1 large and 1 small) for 2 min. After incubating in

256    -20 ℃ for 20 min, we treated our samples with ultrasound in ice bath for 30min and

257    add 1 mL chloroform. After another -20 ℃ incubation for 20 min, we treated our

258    samples with ultrasound in ice bath for 5 min and centrifuged at 15871 g for 5 min

259    before vortexing for 1 min. Then we removed 900 μL of the lower layer (divided in

260    two tubes, each 450 μL) in a 1.5 mL brown LCMS sample vial and dry the samples.

261    We resuspended the sample with 200 μL treatment solution (methanol: water = 4:1)

262    with ultrasound treatment in ice bath for 1 min. Samples were stored at -20 ℃ before

263    going to the machine (The whole process was under low temperature). The mass

264    spectrometry system used the API 5500 Triple Quadrupole Mass Spectrometry

265    System from AB Sciex, USA, with an electrospray (ESI) ion source and an Analyst

266    1.6.2 workstation. The chromatographic system used Waters' ultra-high performance

267    liquid chromatography. The Agilent Poroshell 120, EC-C18 (100*3 mm, 2.7 μm) LC

268    column is used according to the nature of auxin. The injection volume is 3 μL. The

269    default parameters are used in the Analyst software (AB Sciex, USA, version number:

270    1.6.2) to automatically identify and integrate each MRM transition and assist with

271    manual inspection.

272

273    **RESULTS**

274    **Tonoplast proton pumps play an essential role in embryogenesis**

275        We constructed triple mutants lacking both V-ATPase (VHA-a2 and VHA-a3) and

276    V-PPase (AVP1) to investigate functions of tonoplast proton pumps in Arabidopsis.

277    We first crossed two single mutants of *VHA-a2* (SALK_142642) and *VHA-a3*

278    (SALK_029786) to generate double mutant *vha2* , which has the same genotype as

279    previously reported mutant (Krebs *et al*., 2010), but it was rebuilt by us. This double

280    mutant was further crossed, respectively, with two different alleles of *AVP1* gene,

281    *avp1* (Yang *et al*., 2015) and *fugu5-1* (Ferjani *et al*., 2007) to produce two triple

282    mutants *vap3* and *fap3* (Fig. S1a-b). The *fap3* has the same genotype as the mutant

283 described previously (Kriegel *et al*., 2015) but it was rebuilt by us and *vap3* was a

284 new triple mutant allele. Our triple mutants are confirmed by PCR and qRT-PCR (Fig.

285 S1c-d).

286    Phenotypic analysis illustrated *vap3* and *fap3* had abnormal embryogenesis. We

287 examined embryo development of Col and *vap3* and found that 70% of *vap3* ovules

288 failed to develop to one-cell embryo and the others embryos showed various degree of

289 abnormal pattern formation (Fig. 1a-u). The embryos of *vap3* had abnormal

290 embryonic body and abnormal suspensor, as well as stunted or arrested development

291 (Fig. 1v). The embryo development of *fap3* had similar defects with *vap3* (Fig. 1v)

292 and Microscopic analysis of *vap3* mutant embryos at one-cell stage revealed defects

293 from the very beginning of embryogenesis. The wild type embryo contained a round

294 apical cell and a long basal cell after the first horizontal and asymmetrical division.

295 The apical cell was small with thick cytoplasm and eventually developed to the

296 embryo and the basal cell was larger and ultimately developed to suspensor (Mayer *et*

297 *al*., 1993). The *vap3* and *fap3* embryo was defective throughout the development from

298 one-cell to sixteen-cell stages, and subsequently from globular, heart-shaped, to the

299 mature stage (Fig. 1a-u). Starting from early stage, the suspensor cells were shorter

300 and the cell division in some cases was arrested in *vap3* embryos (Fig. 1a-u). At

301 octant stage, the embryo of *vap3* displayed multinuclear cells and unequal

302 cytoplasmic division (Fig. 1g-i). From globular to heart-shaped stage, the symmetrical

303 primordia and intermediate boundaries of the cotyledons were established in the Col

304 embryo, setting the foundation for cotyledons pattern formation (Long *et al*., 1996). In

305 *vap3*, the cotyledon primordia became asymmetric with delayed cell division (Fig.

306 1n-o). We also observed embryogenesis and vacuole morphology of Col, *avp1* and

307 *vha2* (Fig. S2). The embryo development of wild type and *avp1* did not have an

308 abnormal developmental phenotype from one-cell embryo, while a relatively low

309 proportion of *vha2* had abnormal suspensors (Fig. 1v). Very few double mutants

310 (2/187) had abnormal cell division in the late stage of globular embryos (Fig. S2), and

311 these will eventually show abnormal cotyledons after germination. We summarized

312 the abnormal cell division and pattern formation in triple mutants' embryo (Fig. 1w).

**313**

**Vacuole morphology and distribution are several defected during**

**embryogenesis in the mutants lacking tonoplast proton pumps**

A recent study (Kimata *et al*., 2019) suggests that vacuole polar distribution plays an essential role in the first asymmetric division of zygote. Kriegel *et al* (2015) reported that lack of two tonoplast proton pumps may have altered vacuole morphology in the elongation and transition zone of the mutant roots. Taking these studies together, we hypothesized that early embryonic cells in the *fap3* and *vap3* mutants may suffer from altered vacuole morphology that leads to abnormal embryo pattern formation. Using CLSM and Differential Interference Contrast Microscope (DIC), we observed severe defects in the size, shape, and distribution of vacuoles in mutant embryo cells as compared to the wild type (Fig. 1a-c, Fig. 2). After the first division of zygote in the wild type plants, a large vacuole is found in the basal cell while the apical embryonic cell has very small vacuoles (Kimata *et al*., 2019) (Fig. 1a, Fig. 2a). In contrast, at the same stage, the apical cells featured larger vacuoles and the basal cells featured a lot of smaller vacuoles in triple mutants (Fig. 1b-c, Fig. 2b). Subsequently, at four- and eight- and sixteen-cell embryo stages, bigger vacuoles persisted in the embryonic cells whereas smaller vacuoles were found in suspensor cells in the mutant, accompanied by severe defects in cell division and pattern formation throughout these stages (Fig. 2c-i). Using a cartoon sketch, we aligned the vacuole morphology and embryo cell division pattern in Fig. 2j. It becomes clear that the abnormal vacuole morphology and distribution are tightly linked to defective embryo cell division and pattern formation. Together with the recent report (Kimata *et al*., 2019), our results indicated that the abnormal vacuole morphology is causal to defects in embryo cell division and pattern formation.

**Lacking tonoplast proton pump activity results in severe defects in**

**plant morphogenesis**

341       We compared the phenotypes of Col, *avp1*, *fugu5-1*, *vha2*, *vap3* and *fap3* plants

342 during the life cycle and found very little difference in the morphology between the

343 single mutants and the wild type. *vap3*, *fap3* and *vha2*, however, showed strong

344 phenotypic changes as compared to the wild type or single mutant plants. The adult

345 plants of the *vha2*, *vap3* and *fap3* mutants showed severely stunted stature and

346 reproductive defects (Fig. S3). Besides, we found new phenotypic defects of the triple

347 mutants during early seedling development that were not reported previously. In

348 particular, almost all (99%) of *vap3* seedlings showed different degree of cotyledon

349 abnormality (Fig. 3a-m), including deformed two cotyledons, three cotyledons,

350 partially fused cotyledons, and cup-shaped cotyledons (Fig. 3e-h). Another allele, *fap3,*

351 had 90% abnormal cotyledons (Fig. 3i-l). Comparing to triple mutants, a small portion

352 (less 1%) of *vha2* seedlings after germination had obvious abnormal cotyledons

353 (mainly fused cotyledons) (Fig. 3d). Using scanning electron microscopy (SEM), we

354 also found abnormal development of shoot apical meristem (SAM) in *vap3*, in

355 addition to cotyledon defects (Fig. 3n-α).

356       Consistent with the description of *fap3* in previous report (Kriegel *et al*., 2015), the

357 *vap3* and *fap3* seedlings displayed short root phenotype comparing to Col, *avp1*, and

358 *fugu5-1* (Fig. 4a-b). We further examined the root tip anatomy of *vap3* mutant and

359 found disturbed Quiescent Center region and smaller root cap, indicating altered cell

360 division pattern of root meristem (Fig. 4c-n) and root cap (Fig. 4o). We also noted the

361 V-ATPase double mutant *vha2* showed reduced root growth, but *avp1* and *fugu5-1* did

362 not show any significant changes in pattern formation. Apparently, the two tonoplast

363 proton pumps, AVP1 and V-ATPase, may have synergistic functions in the regulation

364 of early plant pattern formation.

365       In addition to defects in root growth, the triple mutants *vap3* and *fap3* showed

366 reduced gravity responses (Fig. S4a-b). Furthermore, *vap3*/*fap3* mutants were

367 apparently less sensitive to exogenous 1-naphthylacetic acid (NAA) (Fig. S4c). When

368 treated with auxin polar transport inhibitor 1-N-naphthylphthalamic acid (NPA), *vha2*,

369 *vap3* and *fap3* were less sensitive to NPA as compared to the wild type and single

370 mutants, implying that auxin polar transport may be affected by the disruption of the

371   vacuolar proton pumps (Fig. S4d). Together, embryo defects and reduced auxin

372   responses supported the hypothesis that lack of vacuolar proton pumps may have

373   altered auxin signaling in the mutant plants.

374

**PIN1 localization and auxin distribution were altered in triple**
375

**mutants**
376

377   Pattern formation during embryogenesis, especially cotyledon initiation and

378   development, is determined by auxin signaling (Gälweiler, 1998). Auxin signaling in

379   plant development is often determined by the accumulation and transport of this

380   hormone within plant organs, which is limited by activities of several distinct families

381   of transporters. In particular, PIN-FORMED (PIN) members play critical roles in

382   polar auxin transport during embryonic and post-embryonic stages, thus tightly

383   controlling plant organogenesis and seedling development. Among the PINs, PIN1 is

384   a major transporter for polar auxin flow during embryogenesis (Vernoux *et al*., 2000).

385   Cotyledon morphology at mature stage of the *fap3* and *vap3* embryos, including fused

386   cotyledons, multiple cotyledons, and asymmetric cotyledons (Fig. 3a-m and Fig. S5a)*,*

387   is highly similar to that in *pin1-11* mutant (Fig. S5b). We thus crossed the PIN1-EYFP

388   marker line with our mutants and compared its localization in the wild type and

389   mutant backgrounds. In the wild type embryos, PIN1-EYFP signal appeared in the

390   plasma membranes of 16/32-cell embryo cells, and localized in the vascular precursor

391   cells and epidermal cell layer of cotyledon primordia after late globular stage (Fig.

392   5a-d, Friml *et al*., 2003; Xiang *et al*., 2011). In mutant background, PIN1-EYFP signal

393   was reduced in intensity in 16/32-cell embryos and heart-shaped embryos, and

394   showed more diffused distribution in torpedo-shaped embryos and cotyledons (Fig.

395   5e-h). Furthermore, we found that PIN1 is mainly distributed in the basal side of

396   plasma membrane in root pericycle cells of wild type plants (Fig. 5i-j). Interestingly,

397   PIN1 protein level was dramatically reduced in *vap3* root (Fig. 5k-l). The

398   Western-Blot and fluorescence intensity of PIN1 in roots were produced to further

399   demonstrate the reduction of total PIN1 protein in *vha2* and *vap3* (Fig. 5m-o).

400    We further examined auxin distribution and accumulation pattern using transgenic

401    plants expressing the β-glucuronidase (GUS) reporter gene driven by synthetic

402    auxin-responsive promoter DR5. The previous reports (Gonzalez, 2010; Li *et al*.,

403    2010) show that auxin content is increased in the transgenic lines overexpressing

404    *AVP1*, indicating that AVP1 activity is positively correlated with auxin content. We

405    found that the GUS signal in *avp1* mutant (Fig. S5c-f) was less intense as compared to

406    that in the wild type, suggesting a disturbed auxin distribution in *avp1*. We measured

407    the auxin content of young rosette leaves in 21-DAG *avp1* plants and indeed found a

408    32% drop of auxin level as compared to the wild type (Table S1). In addition, we also

409    found that distribution of GUS signal was altered in *vha2* (Fig. S5e) and the auxin

410    content was decreased in *vha2* as well (Table S1), suggesting that auxin content and

411    polar transport was affected in *vha2*. In *vap3* triple mutant, the DR5 signal was less

412    intense, the distribution of DR5 signal was significantly changed (Fig. S5f), and the

413    auxin content was decreased (Table S1), suggesting that both auxin content and

414    distribution were affected in triple mutant.

415    To investigate the detailed abnormality of mutant root, we further visualized

416    vacuole morphology in the two developmental zones. The roots were stained with

417    FB28 (Figure 6a), FM4-64 and BCECF-AM (Figure 6b-e). In the elongation zone,

418    wild type root cells start to rapidly expand accompanied by the inflation of vacuoles

419    (Figure 6b-c). And meristematic root cells of wild type roots contained a complex

420    tubular vacuolar network surrounding the nucleus (Figure 6d-e). Vacuole morphology

421    in mutant roots was severely altered, which appeared as multiple spheres of different

422    sizes distributed within the cell (Figure 6b-e) in these two zones, similar to reported

423    phenotypes of *fugu5-1 vha-a2 vha-a3* (Kriegels *et al*., 2015). Based on BCECF-AM

424    staining, the Ratio 488 /458 indicated the vacuole neutralization (Gao *et al*., 2015) in

425    roots of *vap3* (Figure S6).We further extracted the vacuole from protoplast (Figure

426    6f-k) and we found that the diameter of protoplast and vacuole of *vap3* was reduced

427    than Col, indicating the vacuole size and morphology were changed in *vap3*.

428    PIN1 localization was reported to be regulated by vesicular trafficking

429    (Kleine-Vehn and Friml, 2008). We detected the PIN1 localization in WT and mutant

430    background after BFA treatment. Consistent with previous finding in wild type

431    background (Kleine-Vehn *et al*., 2009), PIN1 aggregated into BFA compartments (Fig.

432    6l-m). But PIN1 protein distribution was largely insensitive to BFA-treatment in the

433    mutant background (Fig. 6n-o), suggesting that PIN1 vesicular trafficking may be

434    defective in *vap3* background and thereby causing abnormality of PIN1 polar

435    localization and auxin distribution.

436

437    **Discussion**

438    Our study suggested that AVP1 and VHA-a2/VHA-a3 function in embryo pattern

439    formation    and    subsequent    developmental    processes,    especially    seedling

440    morphogenesis.    In our study, null mutants of V-PPase (*fugu5-1* and *avp1*) had

441    basically normal development process, PIN1 localization and auxin content, which is

442    consistent with Kriegel's result.    Vacuolar proton pumps may be involved in vacuole

443    morphology and distribution that have been shown to be associated with early embryo

444    development. A recent study shows that polar distribution of vacuoles plays a role in

445    the first asymmetric division of zygote (Kimata *et al*., 2019). We found that vacuole

446    morphology in *vap3/fap3* embryo from one-cell stage was altered as compared to the

447    wild type (Fig. 1a-c, Fig. 2a-i), consistent with the possibility that the tonoplast proton

448    pumps function in vacuole morphology and distribution thereby affecting embryo

449    development. We noted that about 70% (*vap3*)-77% (*fap3*) mutant progenies failed to

450    develop to one-cell embryo, indicating earlier stage defects in female gametogenesis,

451    fertilization, and/or first zygote division. This is consistent with the finding by Kimata

452    (Kimata *et al*., 2019) that vacuole morphology is important for the first division of the

453    zygote. In other words, the triple mutants studied here have severe defects in vacuole

454    morphology, leading to failure of 70-77% zygotes to go through the first division. For

455    the 20-30% of the zygotes that did manage to divide, the patterns of cell divisions in

456    subsequent embryogenesis are severely altered thereby resulting in abnormal pattern

457    formation of the survived embryos. The connection between the tonoplast proton

458    pumps and vacuole morphology is logical as the pump activities are the major driving

459    forces for molecular trafficking in and out of vacuoles, controlling turgor pressure and

460    biogenesis of vacuoles.

461        While defects in early embryo development in the mutant may be a result of altered

462    vacuole morphology and cell division pattern, later defects in seedling development

463    may have been caused by changes in the distribution of PIN1. Vacuole morphology

464    and PIN1 localization may be linked through cellular pH regulation that controls

465    protein trafficking in the cells (Geldner *et al*., 2001). Indeed, vacuole morphology and

466    PIN1-EYFP signal in *vap3* root cells were both altered as compared to the wild type

467    (Fig. 5i-l, Fig. 6b-e), suggesting a possible connection between vacuole morphology

468    and PIN1 localization. Lack of proton pump activities directly alters cellular pH

469    homeostasis, leading to higher pH value of vacuole and lower pH value of the

470    cytoplasm, which has been proposed to cause abnormal PIN1 localization (Geldner *et*

471    *al*., 2001). As a result, auxin distribution will change and cause further defects in later

472    embryos and seedling morphology. Indeed, defects in the *vap3* and *fap3* cotyledons

473    lacking both pumps were similar to those in *pin1-11*, *RPS5A≫PID* (Friml *et al*., 2004)

474    and *cuc1 cuc2* (Aida *et al*., 2002)*,* suggesting that these mutants may have severe

475    defects in auxin transport and signaling possibly as a result of changes in PIN1

476    localization (Fig. S5b). As a major efflux carrier of auxin, PIN1 plays a critical

477    function in polar auxin transport (Friml *et al*., 2004; Kleine-Vehn and Friml, 2008).

478    PIN1 protein has been shown to recycle between intracellular compartments and

479    plasma membrane through vesicular trafficking. The processes that govern

480    endocytosis and exocytosis therefore determine the distribution of PIN1 protein and

481    consequently auxin transport. Our results illustrated that the abundance and

482    exocytosis of PIN1 was disturbed in *vap3* (Fig. 7), and subsequently lead to reduced

483    PIN1 abundance in plasma membrane, suggesting that tonoplast proton pumps may

484    function in PIN1 localization that in turn controls auxin distribution and

485    embryo/cotyledon development. This is consistent with an earlier study on the

486    function of cytosolic subunit C (VHA-C) of the V-ATPase (also called

487    DEETIOLATED3, or DET3) (Lamix *et al*., 2008), which suggested that DET3 plays a

488    role in trafficking plasma membrane proteins, such as PIN2 and BRI1 (Luo *et al*.,

2015). Because loss of DET3 increases the pH in the TGN/EEs, but not vacuole, authors concluded that DET3 activity controls pH in TGN/EEs, which in turn regulates vesicular trafficking (Lamix *et al*., 2008). In contrast, loss-of-function of both VHA- and AVP1-type tonoplast proton pumps leads to raised pH of vacuole (Krebs *et al*., 2010; Kriegel *et al*., 2015). Together with our results here, these findings suggested that vacuolar pH may also be important for intracellular trafficking of plasma membrane proteins such as PIN1, to control auxin transportation and distribution.

In conclusion, tonoplast proton pumps play essential roles in vacuole morphology and distribution during embryo cell division and embryo pattern formation. At and after 16/32-cell embryo stages, PIN1 protein polar localization becomes a key determinant for further embryo development. The cellular pH (controlled by vacuolar proton pumps) is a key factor for correct trafficking of plasma membrane proteins including PIN1. As Kriegel's research mentioned, a null mutant of V-PPase (*fugu5-1*) exhibited no change in developmental processes and vacuole pH. In our opinion, we considered that there are two types of proton pumps at tonoplast and they both play the role of transporting $H^+$ into vacuole. If one of them is missing, the other one will also exercise this function (in partial level). In both null mutant of V-PPase (*avp1* or *fugu5-1*) and null mutant of V-ATPases (*vha2*), they have the ability of transporting $H^+$ into vacuole relying on another functional enzyme. But for *vap3* or *fap3*, they lost the function of both two types of proton pumps. It is very reasonable that triple mutant has severe phenotypes. Our hypothesis seemed to be similar to "share work model" raised in Kriegel's paper (Kriegel *et al*., 2015).

Lacking tonoplast proton pumps thus would cause severe defects in embryo patterning due to altered vacuolar morphogenesis and pH control (Fig. 7).

## ACKNOWLEDGMENTS

525

## AUTHOR CONTRIBUTION

527

528  W.L. designed the study, performed experiments, analyzed data, wrote and

529  modified the manuscript, and acquired funding. S.L. designed the study, wrote and

530  modified the manuscript, and acquired funding. Y.J. performed experiments and wrote

531  the manuscript. R.T. performed experiments, Y.Z. helped analyzed data. H.X. helped

532  organized the results. A.F. offered the materials and helped organized the results and

533  the manuscript. All authors agree to be accountable for the content of this paper.

534

## Reference

536  **Aida M, Vernoux T, Furutani M, Traas J, Tasaka M. 2002.** Roles of

537  PIN-FORMED1 and MONOPTEROS in pattern formation of the apical region of

538  the Arabidopsis embryo. Development **129**: 3965-3974.

539  **Cipriano DJ, Wang Y, Bond S, Hinton A, Jefferies KC, Qi J, Forgac M,2008.**

540  Structure and regulation of the vacuolar atpases. *Biochim Biophys Acta* **1777**:

541  599-604.

542  **Christensen CA, King EJ, Jordan JR, Drew GN. 1997.** Megagametogenesis

543  inArabidopsiswild type and theGfmutant. *Sexual Plant Reproduction* **10(1)**:49-64.

544  **Dettmer J, Hong-Hermesdorf A, Schumacher K. 2006.** Vacuolar $H^+$-atpase activity

545  is required for endocytic and secretory trafficking in Arabidopsis. *The Plant Cell* **18**:

546  715-730.

547  **Drozdowicz Y, Rea P. 2001.** Vacuolar H$^+$ pyrophosphatases: from the evolutionary

548  backwaters into the mainstream. *Trends in Plant Science* **6**:206-211.

549  **Ferjani A, Segami S, Horiguchi G, Muto Y, Maeshima M, Tsukaya H. 2011.**

550  Keep an eye on PPi: the vacuolar-type H$^+$-pyrophosphatase regulates

551  postgerminative development in Arabidopsis. *The Plant Cell* **23**: 2895-2908.

552  **Ferjani A, Horiguchi G, Yano S, Tsukaya H. 2007.** Analysis of leaf development in

553  fugu mutants of Arabidopsis reveals three compensation modes that modulate cell

554  expansion in determinate organs. *Plant Physiology* **144**: 988-999.

555  **Friml J, Vieten A, Sauer M, Weijers D, Schwarz H, Hamann T, Offringa R,**

556  **Jürgens G. 2003.** Efflux-dependent auxin gradients establish the apical–basal axis

557  of *Arabidopsis*. Nature 426: 147.

558  **Friml J, Yang X, Michniewicz M, Weijers D, Quint A, Tietz O, Benjamins R,**

559  **Ouwerkerk PB, Ljung K, Sandberg G** *et al*. **2004.** A PINOID-dependent binary

560  switch in apical-basal PIN polar targeting directs auxin efflux. *Science* **306**:

561  862-865.

562  **Gonzalez N, De Bodt S, Sulpice R, Jikumaru Y, Chae E, Dhondt S, Van Daele T,**

563  **De Milde L, Weigel D, Kamiya Y** *et al*. **2010.** Increased leaf size: different means

564  to an end. *Plant physiology* **153**: 1261-1279.

565  **Geldner N, Friml J, Stierhof YD, Jürgens G, Palme K. 2001.** Auxin transport

566  inhibitors block PIN1 cycling and vesicle trafficking. *Nature* **413**: 425.

567  **Gälweiler L, Guan C, Müller A, Wisman E, Mendgen K, Yephremov A, Palme K.**

568  **1998.** Regulation of polar auxin transport by AtPIN1 in Arabidopsis vascular tissue.

569  *Science* **282**: 2226-2230.

570  **Gaxiola RA, Li J, Undurraga S, Dang LM, Allen GJ, Alper SL, Fink GR. 2001.**

571  Drought- and salt-tolerant plants result from overexpression of the AVP1 H$^+$-pump.

572  *Proc Natl Acad Sci U S A* **98.20**:11444-11449.

573  **Gao Y, Zhou H, Chen J, Jiang X, Tao S, Wu J, Zhang S. 2015.** Mitochondrial

574  dysfunction mediated by cytoplasmic acidification results in pollen tube growth

575  cessation in\r, *pyrus pyrifolia*. *Physiologia Plantarum,* **153(4)**, 603-615.

576  **Herman EM, Li X, Su RT, Larsen P, Hsu H, Sze H. 1994.** Vacuolar-type H$^+$

577    -ATPases are associated with the endoplasmic reticulum and provacuoles of root tip

578    cells. *Plant Physiology* **106**: 1313-1324.

579    **Kriegel A, Andrés Z, Medzihradszky A, Krüger F, Scholl S, Delang S,**

580    **Patir-Nebioglu MG, Gute G, Yang H, Murphy AS *et al*. 2015.** Job Sharing in the

581    Endomembrane System: Vacuolar Acidification Requires the Combined Activity of

582    V-ATPase and V-PPase. *The Plant cell* **27**: 3383-96.

583    **Krebs M, Beyhl D, Esther Görlich, Al-Rasheid KAS, Schumacher K. 2010.**

584    Arabidopsis V-ATPase activity at the tonoplast is required for efficient storage but

585    not for sodium accumulation. *Proceedings of the National Academy of Sciences*

586    **107**: 3251-3256.

587    **Kleine-Vehn J, Friml J. 2008.** Polar targeting and endocytic recycling in

588    auxin-dependent plant development. *Annual review of cell and developmental*

589    *biology* **24**: 447-473.

590    **Kleine-Vehn J, Huang F, Naramoto S, Zhang J, Michniewicz M, Offringa R,**

591    **Friml J. 2009.** PIN auxin efflux carrier polarity is regulated by PINOID

592    kinase-mediated recruitment into GNOM-independent trafficking in Arabidopsis.

593    *The Plant Cell* **21**: 3839-3849.

594    **Kimata Y, Kato T, Higaki T, Kurihara D, Yamada T, Segami S, Morita MT,**

595    **Maeshima M, Hasezawa S, Higashiyama T *et al*. 2019.** Polar vacuolar

596    distribution is essential for accurate asymmetric division of Arabidopsis zygotes.

597    *Proceedings of the National Academy of Sciences* **116**: 2338-2343.

598    **Kurihara D, Mizuta Y, Sato Y, Higashiyama T. 2015.** ClearSee: a rapid optical

599    clearing reagent for whole-plant fluorescence imaging. *Development* **142**:

600    4168-4179.

601    **Li Z, Baldwin CM, Hu Q, Liu H, Luo H. 2010.** Heterologous expression of

602    Arabidopsis $H^+$-pyrophosphatase enhances salt tolerance in transgenic creeping

603    bentgrass (Agrostis stolonifera L.). *Plant, Cell & Environment* **33**: 272-289.

604    **Long JA, Moan EI, Medford JI, Barton MK. 1996.** A member of the KNOTTED

605    class of homeodomain proteins encoded by the STM gene of Arabidopsis. *Nature*

606    **379**: 66.

607   **Laxmi A, Pan J, Morsy M, Chen R. 2008.** Light plays an essential role in

608         intracellular distribution of auxin efflux carrier PIN2 in Arabidopsis thaliana. *PloS*

609         *one* **3**: e1510.

610   **Luo Y, Scholl S, Doering A, Zhang Y, Irani NG, Rubbo SD, Neumetzler L,**

611         **Krishnamoorthy P, Van Houtte I, Mylle E *et al*. 2015.** V-ATPase activity in the

612         TGN/EE is required for exocytosis and recycling in Arabidopsis. *Nature plants*

613         **1**:15094.

614   **Li J, Yang H, Peer WA, Richter G, Blakeslee J, Bandyopadhyay A,**

615         **Titapiwantakun B, Undurraga S, Khodakovskaya M, Richards EL *et al*. 2005.**

616         Arabidopsis $H^+$-PPase AVP1 regulates auxin-mediated organ development. *Science*

617         **310**: 121-125.

618   **Murashige T, Skoog F. 1962.** A revised medium for rapid growth and bio assays with

619         tobacco tissue cultures. *Physiologia plantarum* **15**: 473-497.

620   **Maeshima M. 2001.** Tonoplast transporters: organization and function. *Annu Rev*

621         *Plant Physiol Plant Mol Biol* **52**: 469-497.

622   **Nelson N. 2003.** A journey from mammals to yeast with vacuolar $h^+$-atpase (v-atpase).

623         *Journal of Bioenergetics and Biomembranes* **35**: 281-289.

624   **Nishi T, Forgac M. 2002.** The vacuolar $(H^+)$-ATPases--nature's most versatile proton

625         pumps. *Nature Reviews Molecular Cell Biology* **3**: 94-103.

626   **Neuhaus HE, Trentmann O. 2014.** Regulation of transport processes across the

627         tonoplast[J]. *Frontiers in Plant Science* **5**:460.

628   **Oberbeck K, Drucker M, Robinson DG. 1994.** V-type ATPase and pyrophosphatase

629         in endomembranes of maize roots. *Journal of Experimental Botany* **45**: 235-244.

630   **Sabatini S, Beis D, Wolkenfelt H, Murfett J, Guilfoyle T, Malamy J, Benfey P,**

631         **Leyser O, Bechtold N, Weisbeek P *et al*. 1999.** An auxin-dependent distal

632         organizer of pattern and polarity in the Arabidopsis root. *Cell* **99**: 463-472.

633   **Segami S, Nakanishi Y, Sato MH, Maeshima M. 2010.** Quantification,

634         Organ-Specific Accumulation and Intracellular Localization of Type II

635         $H^+$-Pyrophosphatase in Arabidopsis thaliana. *Plant & Cell Physiology*

636         **51(8)**:1350-60.

637   **Sze H, Schumacher K, Müller ML, Padmanaban S, Taiz L. 2002.** A simple
638      nomenclature for a complex proton pump: VHA genes encode the vacuolar
639      $H^+$-ATPase. *Trends in Plant Science* **7(4)**:157-161.

640   **Steinmann T, Geldner N, Grebe M, Mangold S, Jackson CL, Paris S, Gälweiler L,**
641      **Palme K, Jürgens G. 1999.** Coordinated polar localization of auxin efflux carrier
642      PIN1 by GNOM ARF GEF. *Science* **286**:316-318.

643   **Vernoux T, Kronenberger J, Grandjean O, Laufs P, Traas J. 2000.** PIN-FORMED
644      1 regulates cell fate at the periphery of the shoot apical meristem. *Development*
645      **127(23)**:5157-65.

646   **Viotti C, Krüger F, Krebs M, Neubert C, Fink F, Lupanga U, Scheuring D,**
647      **Boutté Y, Frescatada-Rosa M, Wolfenstetter S *et al*. 2013.** The endoplasmic
648      reticulum is the main membrane source for biogenesis of the lytic vacuole in
649      Arabidopsis. *The Plant Cell* **25**:3434-49.

650   **Xu J, Hofhuis H, Heidstra R, Sauer M, Friml J, Scheres B. 2006.** A molecular
651      framework for plant regeneration. *Science* **311**: 385-388.

652   **Yang Y, Tang RJ, Mu B, Ferjani A, Shi J, Zhang H, Zhao F, Lan WZ, Luan S**
653      **2018.** Vacuolar Proton Pyrophosphatase Is Required for High Magnesium
654      Tolerance in *Arabidopsis. International journal of molecular sciences* **19**:3617.

655   **Yang Y, Tang RJ, Li B, Wang HH, Jin YL, Jiang CM, Bao Y, Su HY, Zhao N, Ma**
656      **XJ. 2015.** Overexpression of a Populus trichocarpa $H^+$-pyrophosphatase gene
657      *PtVP1. 1* confers salt tolerance on transgenic poplar. *Tree physiology* **35**: 663-677.

658

659

660    **Supporting Information**

661    **Fig. S1 Identification of triple mutant *vap3* and *fap3*.**

662    **Fig. S2 Embryogenesis of *avp1* and *vha2*.**

663    **Fig. S3 Defected growth and development in *vap3*.**

664    **Fig. S4 *vap3/fap3* has disturbed auxin responses.**

665    **Fig. S5 Auxin related phenotypes in *vap3/fap3* and *pin1-11*.**

666    **Fig. S6 Relative vacuole pH measurement of meristem zone and elongation zone**
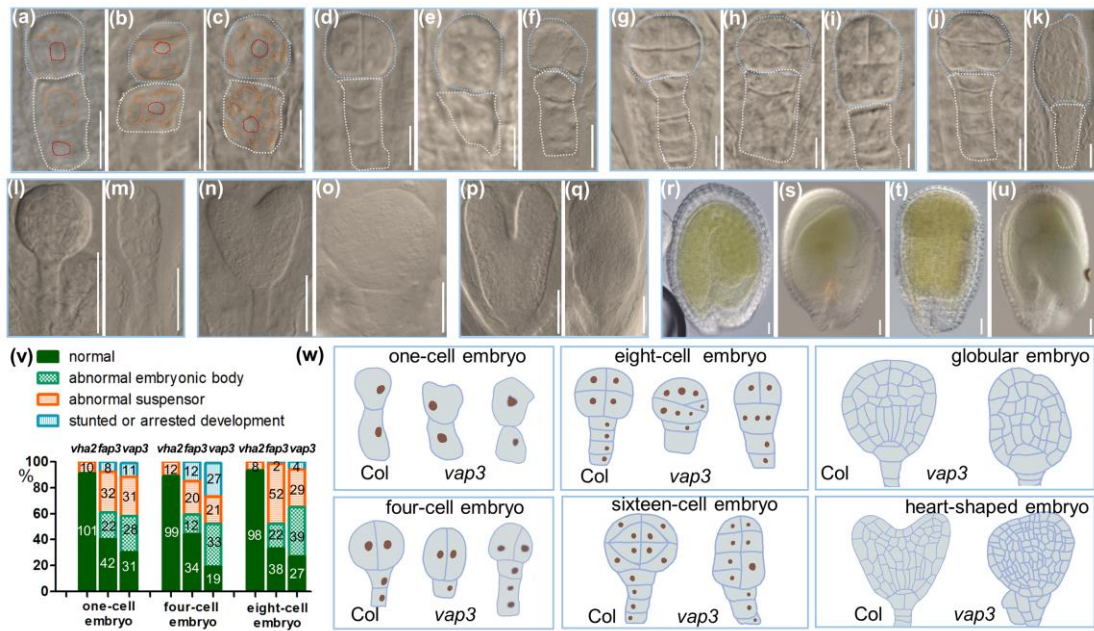
667    **in Col and *vap3* 6-DAG-seedlings roots.**

668    **Table S1 Detection of auxin content of 21-DAG-seedlings of Col, *avp1*, *vha2*,**

669    ***vap3*.**

670

671

**Figure Legend**



**Fig. 1 Abnormal embryogenesis of Arabidopsis mutant *vap3*.**

(a-k) One-cell, four-cell, eight-cell, and sixteen-cell embryos of Col (a, d, g, j) and

*vap3* (b-c, e-f, h-i, k) (bar = 10 μm). The blue lines indicate embryos, the white lines

indicate suspensors, the red lines indicate nuclei of embryo cells, and the orange lines

indicate vacuoles. (l-q) Globular, heart-shaped, and torpedo-shaped embryos of Col (l,

n, p) and *vap3* (m, o, q) (bar = 50 μm). (r-u) Cotyledon embryos of Col (r) and *vap3*

(s-u) (bar = 50 μm). Graphs represent the typical phenotype of all samples (n=100 in

each developmental stage of each line). (v) Phenotypic analysis of abnormal pattern

formations in embryos of Col, *avp1*, *fugu5-1*, *vha2*, *vap3*, *fap3*. Sample numbers are

labeled in each column. (w) The illustration of abnormal pattern formation of *vap3*

embryos. Schematic diagrams of one-cell to heart-shaped embryos showed the

abnormal embryonic body and suspensor, which could be traced to (a-o).

686
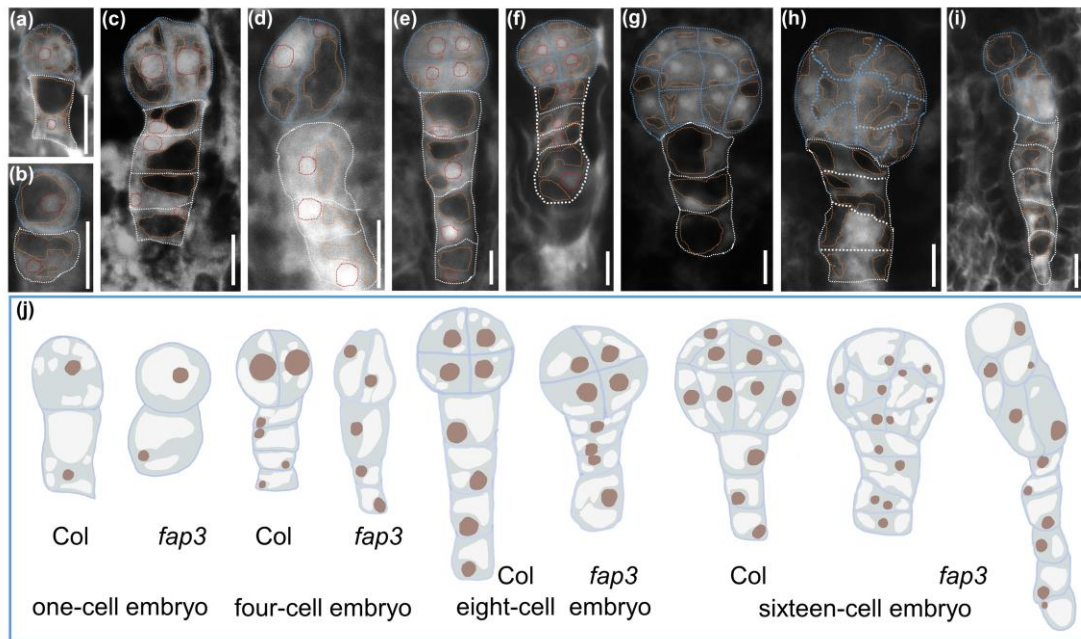
**Fig. 2 Abnormal vacuole morphology and distribution of Arabidopsis mutant**

*fap3*.

(a-b) One-cell embryo of Col (a) and *fap3* (b). Bar = 10 μm. (c-i) four-cell, eight-cell,

and sixteen-cell embryos of Col (c, e, g) and *fap3* (d, f, h-i) (bar = 10 μm). Graphs

represent the typical phenotype of all samples (n=20 in each developmental stage of

Col and *fap3*). (j) The illustration of abnormal vacuole morphology and distribution of

*fap3* embryos. (a-i) The blue lines indicate embryo cells, the white lines indicate

suspensor cells, the red lines indicate nuclei of embryo cells, and the orange lines

indicate vacuoles. Schematic diagrams of one-cell to sixteen-cell embryos showed the

abnormal embryonic body and suspensor, which could be traced to (a-i).

698
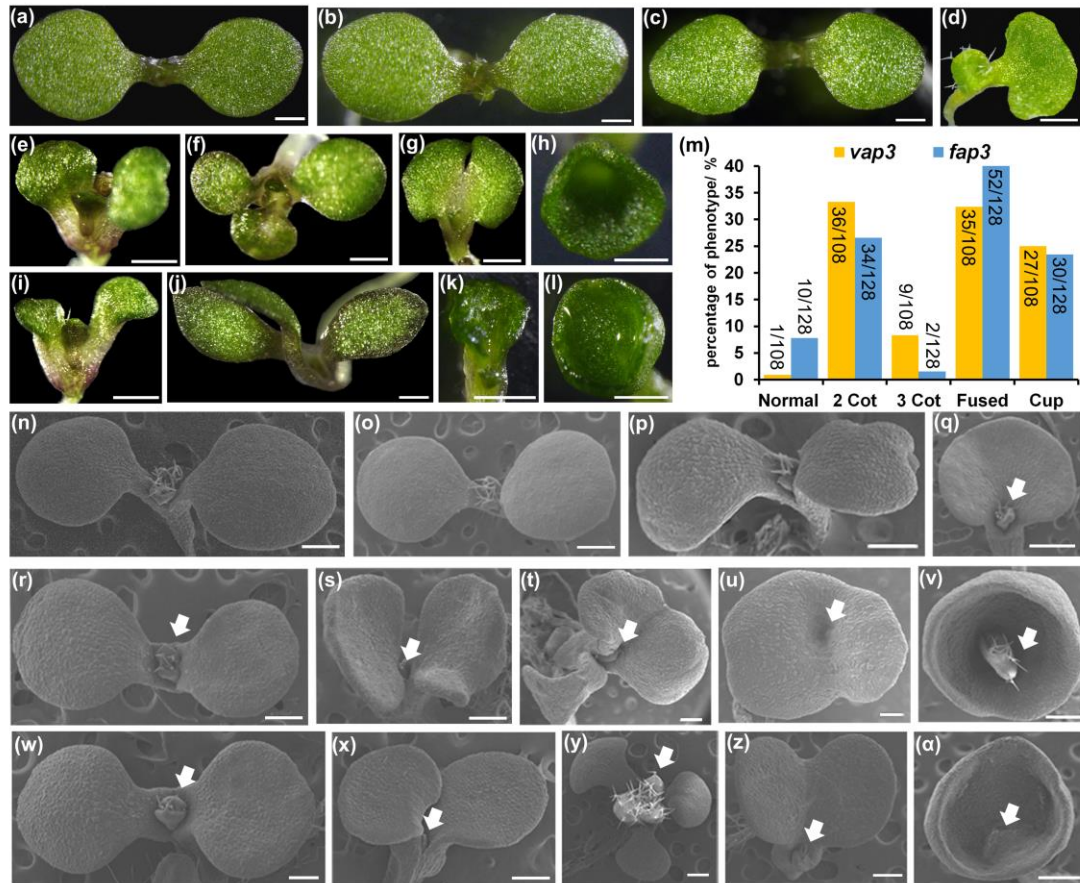
**Fig. 3 Abnormal cotyledons morphology in Arabidopsis mutants *vap3/fap3*.**

Cotyledons in 6-DAG-seedling of (a) Col, (b) *avp1*, (c) *fugu5-1*, (d) *vha2*, (e-h) *vap3*,
(i-l) *fap3* (bar = 500 μm). (m) Phenotypic analysis of different cotyledon phenotypes
of *vap3* and *fap3*. 2 Cot represent abnormal 2 cotyledons, 3 Cot represent abnormal 3
cotyledons, fused represent partially fused cotyledon, cup represent cup-shaped
cotyledon. Sample numbers are labeled in each column. Shoot Apical Meristems in (n)
Col, (o) *avp1*, (p) *fugu5-1*, (q) *vha2*, (r-v) *vap3*, (w-α) *fap3* (bar = 500 μm). Arrows
mark the SAM of seedlings. Graphs represent the typical phenotype of all samples
(n=100 for each line).

708
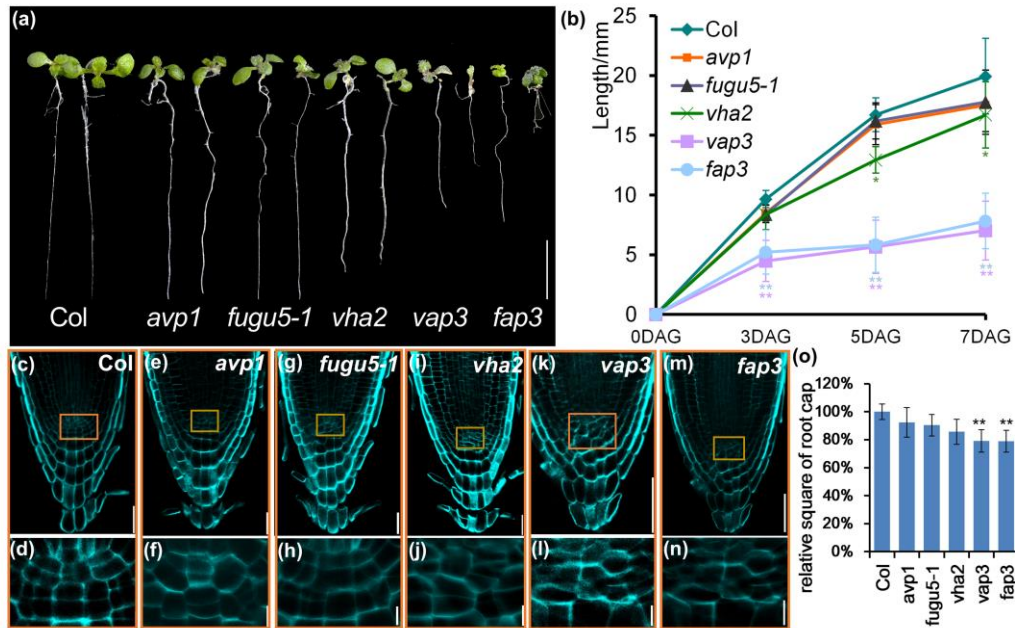
**Fig. 4 Abnormal root development in Arabidopsis mutants *vap3/fap3*.**

(a) Root length of Col, *avp1*, *fugu5-1*, *vha2*, *vap3* and *fap3*. For a more obvious

comparison, the picture shows the 9-DAG-seedling. Graphs represent the typical

phenotype of all samples (n=100 for each line). (b) Statistical analysis of root length.

Bars represent the means ± SD of three biological replicates (n = 30). Asterisks

indicate the significant difference (Student's two tailed t test, *P < 0.05; **P < 0.01).

QC region of Col (c-d), *avp1* (e-f), *fugu5-1* (g-h), *vha2* (i-j), *vap3* (k-l) and *fap3* (m-n)

(bar = 30 μm for c, e, g, i, k, m, and 10 μm for d, f, h, j, l, n). Graphs represent the

typical phenotype of all samples (n=15 for each line). (o) Statistical analysis of

relative square of root cap. Bars represent the means ± SD of three biological

replicates (n = 10). Asterisks indicate the significant difference (Student's two tailed t

test, *P < 0.05; **P < 0.01).

721
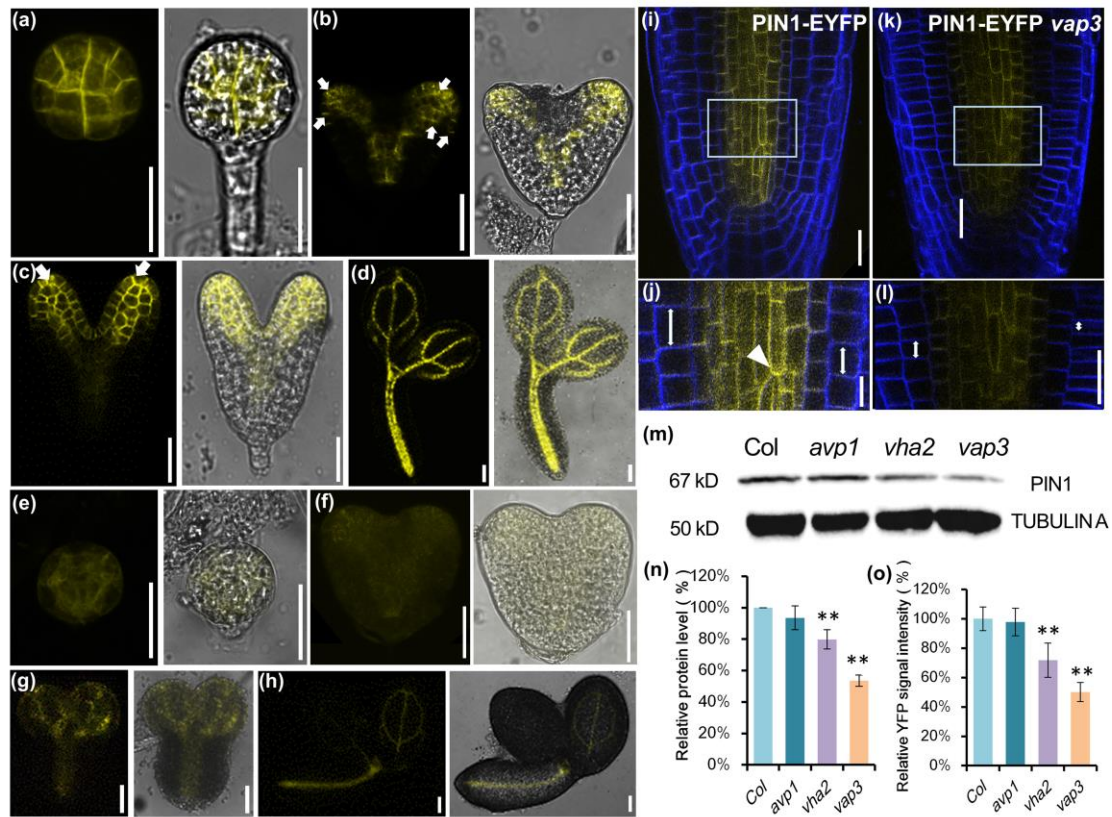
**Fig. 5 Arabidopsis mutant *vap3* has disturbed auxin polar transportation and distribution.**

(a-h) PIN1 level and localization in Col (a-d) and *vap3* (e-h) during embryogenesis (bar = 50 μm). Graphs represent the average intensity of fluorescence of PIN1 protein in embryos. (i-l) PIN1 level and localization in Col (i, j) and *vap3* (k, l) of 5-DAG-seedlings (bar = 30 μm for i and k; and 10 μm for j and l). Arrows mark the localization of PIN1 protein. (m) PIN1 protein level in roots of Col, *avp1*, *vha2* and *vap3*. (n) A quantitative analysis of PIN1 protein levels is shown below and each bar corresponds with the PIN1 band in the blot. Values correspond to the arithmetic means ±SD of three biological replicates (n = 3). Asterisks indicate the significant difference (Student's two-tailed t test, *P < 0.05; **P < 0.01). (o) Relative PIN1-YFP signal intensity in Col, *avp1*, *vha2* and *vap3*. The data are extracted from normalized mean grey levels of PIN1-YFP in Col, *avp1*, *vha2* and *vap3*. Values correspond to the arithmetic means ±SD of three biological replicates (n = 20). Asterisks indicate the significant difference (Student's two tailed t test, *P < 0.05; **P < 0.01).

738
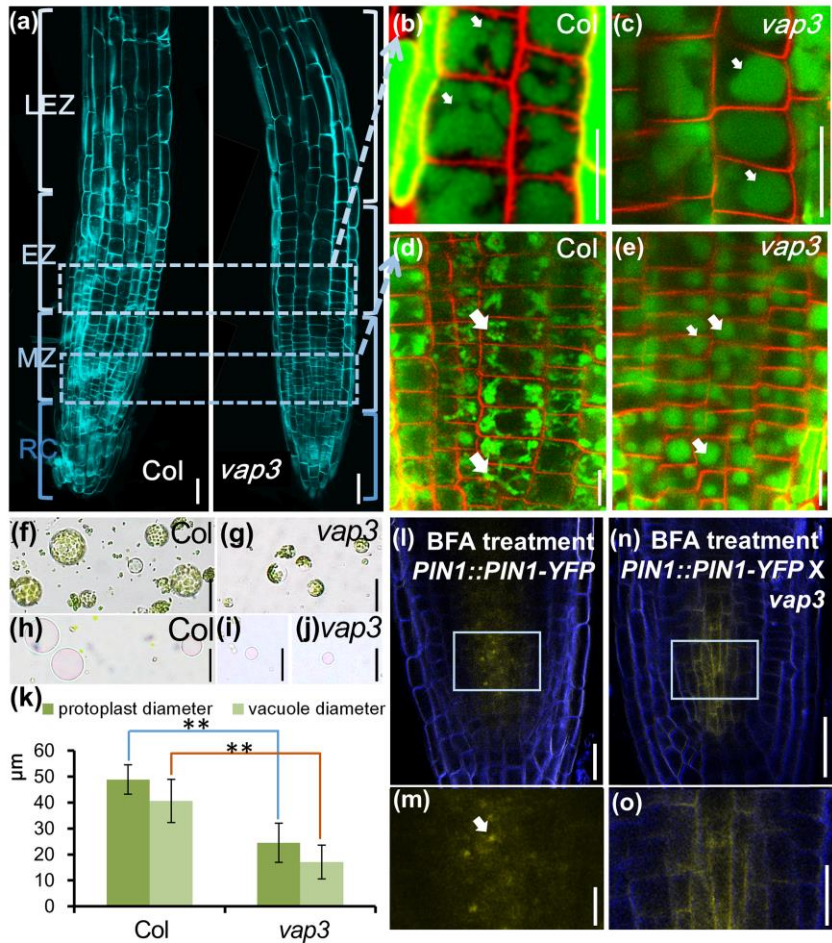
**Fig. 6 Arabidopsis mutant *vap3* has abnormal cell division, vacuole morphology and vesicular trafficking of PIN1 in roots.**

(a) The root pattern of Col and *vap3* (bar = 100 μm). Roots were stained with FB28 (blue). The shape of vacuoles was monitored in the root elongation zone (b-c), and meristematic zone (d-e) of 5-DAG-seedlings of (b, d) Col and (c, e) *vap3*. Roots were stained with BCECF (green) and FM4-64 (red). Arrows mark the different vacuoles. Graphs represent the typical phenotype of all samples (n=15 for each line). Isolated protoplasts of Col (f) and *vap3* (g). Crude vacuoles of Col (h) and *vap3* (i, j) stained with Neutral Red. (k) Statistical analysis of protoplast and vacuole diameters of Col and *vap3*. Bars represent the means ±SD of three biological replicates (n = 30). Asterisks indicate the significant difference (Student's two tailed t test, *P < 0.05; **P < 0.01). PIN1 level and localization in Col (l, m) and *vap3* (n, o) root after BFA treatment (bar = 30 μm for l, n; and 10 μm for m and o). Arrows mark the BFA

752 compartments. Graphs represent the average intensity of fluorescence of PIN1 protein

753 in roots (n=15 for each line).



754
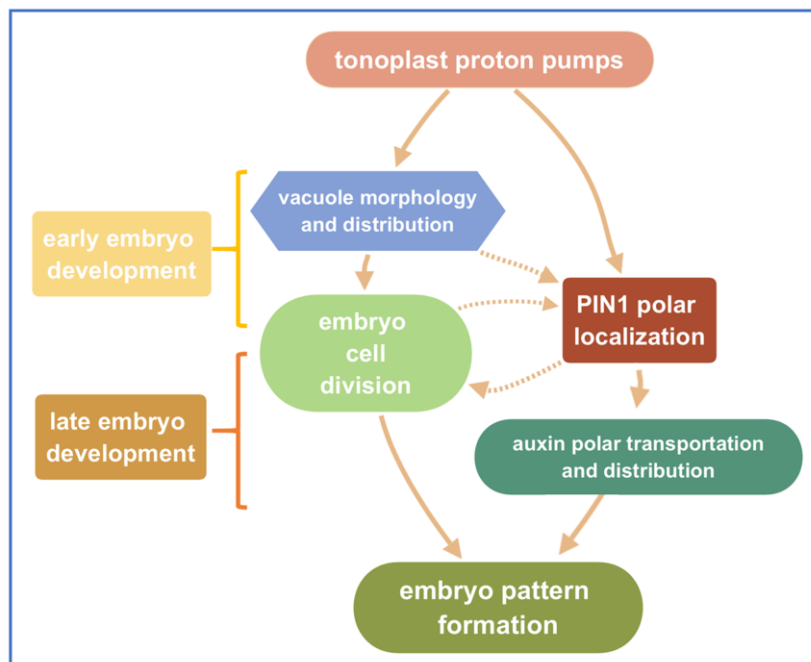
**Fig. 7 The hypothesis model of proton pumps at tonoplast regulating embryo**

756 **pattern formation in Arabidopsis.**

757